Ab initio molecular dynamics simulations of the ferroelectric-paraelectric phase transition in sodium nitrite

Johannes P. Dürholt* and Rochus Schmid†

Computational Materials Chemistry Group, Fakultät für Chemie und Biochemie, Ruhr-Universität Bochum, Bochum 44801, Germany

(Received 14 February 2019; published 19 September 2019)

This paper reports on the first *ab initio* molecular dynamics study of the ferroelectric sodium nitrite, shedding light on its ferroelctric-paraelectric phase transition. The remnant polarization P_r was calculated using a Mulliken population analysis and maximally localized Wannier functions. Especially the Wannier based model is in outstanding agreement with experimental findings and previous Berry phase calculations. The simulations predict a ferroelectric Curie temperature T_c between 425 and 450 K in excellent agreement with the experimental value of 437 K. In addition, the anomalous lattice behavior (shrinking of the c axis) during the phase transition is reproduced. Furthermore, the analysis of the phase transition revealed a combined displacive and order-disorder mechanism. The crystal field effect in the material could be quantified by investigating the molecular dipoles based on the maximally localized Wannier functions and the intermolecular charge transfer by analyzing the Mulliken charges. In agreement with earlier experimental and theoretical findings, the polarization reversal mechanism was found to be dominated by a c-axis rotation of the nitrite ions. The molecular insight into such a simple and prototypical material serves as a basis for a further development of more complex crystalline ferroelectrics, using a design principle inspired by $NaNO_2$.

DOI: 10.1103/PhysRevMaterials.3.094408

I. INTRODUCTION

Ferroelectric materials posses a remnant electric polarization P_r, which can be reversed by the application of an external electric field [1]. They are of interest for technological applications in areas such as data storage, (ultrasound) sensing and actuation, energy harvesting, and optoelectronics [2–4]. Ferroelectricity was observed in different materials like Ceramics [5], polymers [6], molecular crystals [7], and hybrid organic-inorganic materials [8,9]. In recent years, efforts were made to incorporate ferroelectricity in emerging designer materials like metal-organic frameworks (MOFs) [10,11]. For this purpose, often the Perovskite-type ferroelectricity is mimicked [12]. Recently, we introduced the design strategy of rotatable, dipolar, organic linkers to tune the electric field response of MOFs [13]. This strategy could also be used to imitate the concept of prototypical order-disorder ferroelectrics like sodium nitrite ($NaNO_2$) [14].

$NaNO_2$ has a body centered orthorhombic structure (space group $Im2m$), with the dipole vector of the V-shaped nitrite anions aligned parallel to the crystallographic b direction, as shown in Fig. 1. Its remnant polarization P_r stems on the one hand from this ordering of the NO_2^- ions and on the other hand from a translation of the sodium atoms relative to the nitrites. The ferroelectric-paraelectric phase transition occurs at about 437 K. Also the paraelectric phase is orthorhombic (space group $Immm$) with the dipoles disordered with respect to the b axis. An incommensurate, antiferroelectric phase exists in a narrow temperature window from 435 to 437 K. $NaNO_2$ melts at 550 K. The phase transition is accompanied by an anomalous behavior of the lattice constants: when heating the material, the c axis shrinks [15].

Sekhar and coworkers showed that it is possible to tune the ferroelectric properties of the material towards a higher remnant polarization P_r and a higher Curie temperature T_c by incorporation into a poly(vinyl alcohol) film [16,17], which could be used for the fabrication of microelectronic devices.

In order to understand the origin of its ferroelectricity, already in the eighties first theoretical models for $NaNO_2$ were proposed [18]. Massidda and Mirasso showed that for an orthorhombic body-centered lattice of dipoles like $NaNO_2$, the most stable configuration is of ferro type, depending on the choice of the lattice parameters, whereas in an simple orthorhombic lattice it is always of antiferro type [19]. Early molecular dynamics (MD) simulations with Born-Mayer pair potentials were not able to reproduce the ferroelectric low-temperature phase [20–23]. At first in 2003, Yin *et al.* were able to perform MD simulations, which successfully predicted the low-temperature ferroelectric phase [24]. For this purpose they employed pair potentials with a rigid-ion model that was based on Gordon-Kim electron gas theory. Unfortunately, predicted properties like the ferroelectric Curie temperature T_C differed by up to 100 K depending on the chosen model parameters. Furthermore, polarization effects were not included in the model. At the same time, several other groups were trying to model $NaNO_2$ by really predictive but static *ab initio* calculations [25,26]. For example, Alfredsson *et al.* calculated P_r using three different models based on point charges, a multipolar expansion of the charge distribution and the Berry phase approach using Hartree-Fock and LDA

*johannes.duerholt@rub.de
†rochus.schmid@rub.de

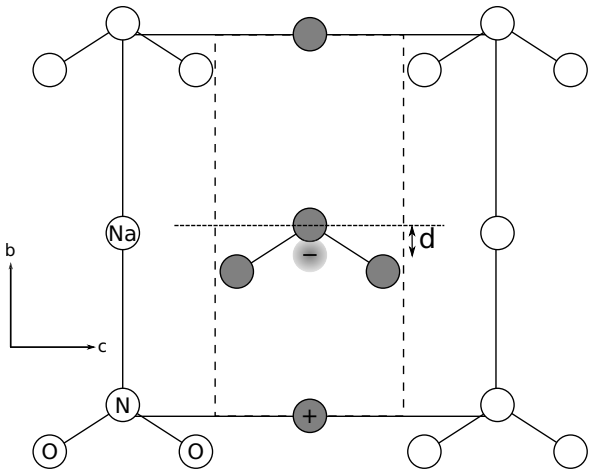

FIG. 1. Schematic representation of the unit cell of $NaNO_2$ in the ferroelectric phase projected along the a axis. The shaded atoms are positioned at $x = \pm 0.5$. The atoms/sites in between the vertical dotted lines represent in analogy to Ref. [31] a one-dimensional chain of alternating cations (sodium atoms) and anions (nitrite ions are mapped on negatively charged sites). The anions are displaced by a distance d relative to the cations, with the horizontal dotted line indicating $\frac{1}{2}b$ and the expected position of a nonpolarized chain ($d = 0$).

Hamiltonians [27]. They found that the Berry-phase approach at the Hartree-Fock level gives a value of 12.0 $\mu C\,cm^{-2}$ for the experimental structure, which is very close to the measured value ($\approx$11.9 $\mu C\,cm^{-2}$ [28] or $\approx$11.7 $\mu C\,cm^{-2}$ [29]).

In the meantime, computational power has increased significantly and more efficient codes like CP2K [30] have been developed, allowing to simulate larger systems for longer timescales by means of *ab initio* molecular dynamics (AIMD) simulations. In this study, we used this approach to perform the first AIMD simulations of the ferroelectric-paraelectric phase transition in $NaNO_2$, combining the high accuracy and predictive power of static first-principles calculations with the insights from MD simulations of a larger supercell of the material. In contrast to perovskite systems, much longer simulation times are needed to simulate the phase transition in $NaNO_2$, since the rotation of a NO_2^- anion happens at much slower timescales in comparison to a lateral atomic displacement in a perovskite system. As a consequence, we sampled in total more than 1.3 ns. Based on this extensive data, we were able to analyze the evolution of P_r and of the cell constants during the phase transition and to analyze the polarization reversal mechanism. Furthermore we quantified the crystal field effect in $NaNO_2$, in order to address the question how the dipole moments of the individual NO_2^- ions change during the phase transition.

II. COMPUTATIONAL DETAILS

AIMD simulations of a $3 \times 3 \times 3$ supercell of $NaNO_2$ (216 atoms) were performed with Born-Oppenheimer dynamics, employing density functional theory (DFT) [32] for the calculation of the energy and atomic forces [33] using the

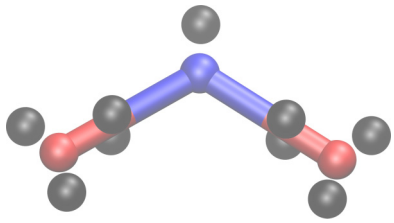

FIG. 2. Nitrite ion in the Wannier representation. Color code: nitrogen (blue), oxygen (red), and Wannier center (black).

QUICKSTEP/CP2K package [30], which is based on a hybrid Gaussian plane-wave approach.

The gradient-corrected PBE functional [34] was used with an empirical correction for the dispersive interactions utilizing the "D3" method by Grimme and coworkers [35]. TZV2P basis sets were employed for Nitrogen and Oxygen atoms whereas the sodium atoms were represented by the DZVP MOLOPT SR basis set [36]. The nine outer electrons of Na were treated explicitly, whereas for all other atoms, only the valence electrons were included. The interaction between core and valence electrons was represented by Goedecker-Teter-Hutter (GTH) type pseudopotentials [37–39]. Following the study by Haigis *et al.* on challenges in first-principles NPT simulations using QUICKSTEP/CP2K, a rather high plane-wave cutoff E_{cut} of 600 Ry together with a relative cutoff E_{cut}^{rel} of 60 Ry was used [40]. Given the systems' size, the Brillouin zone was sampled at the Γ point only.

The system was simulated at 8 different temperatures (77, 150, 198, 250, 298, 350, 400, and 450 K) always starting from the ferroelectric phase using the structure, provided by the materials project [41,42]. At each temperature, the system was first equilibrated for at least 5 ps in the canonical ensemble (NVT) using a CSVR [43] thermostat with a time constant of 100 fs to control the temperature. Then it was further simulated in the NPT ensemble using the same thermostat settings as in the equilibration together with the MTK barostat [44] employing a time constant of 1000 fs to obtain an average pressure of 1 bar. In general, a time step of 0.5 fs was used. The overall simulation time per temperature depends on the closeness to T_c. Equilibration was monitored by the change in P_r along the trajectory [Fig. S1 in Ref. [45] shows the time evolution of P_r along the individual trajectories]. If not stated explicitly, statistical errors for ensemble averages were calculated by performing a reblocking analysis [46]. To further analyze the behavior of $NaNO_2$ close to T_c, an additional simulation was conducted at 425 K by restarting from the simulation at 400 K and ramping up the temperature.

To obtain the remnant polarization of the simulation cell and the ionic dipole moments, maximally localized Wannier functions (MLWFs) were calculated on-the-fly at every tenth time step from the valence orbitals [31,33]. In the Wannier picture, every sodium ion has a charge of 9 e and is tetrahedrally surrounded by four Wannier centers of charge -2 e. A nitrite ion in the Wannier representation is shown in Fig. 2. In addition, point charges were computed by Mulliken population analysis (MPA).

Both for the point charge model and for the Wannier representation, the dipole moment of each ionic species $\vec{\mu}$ was

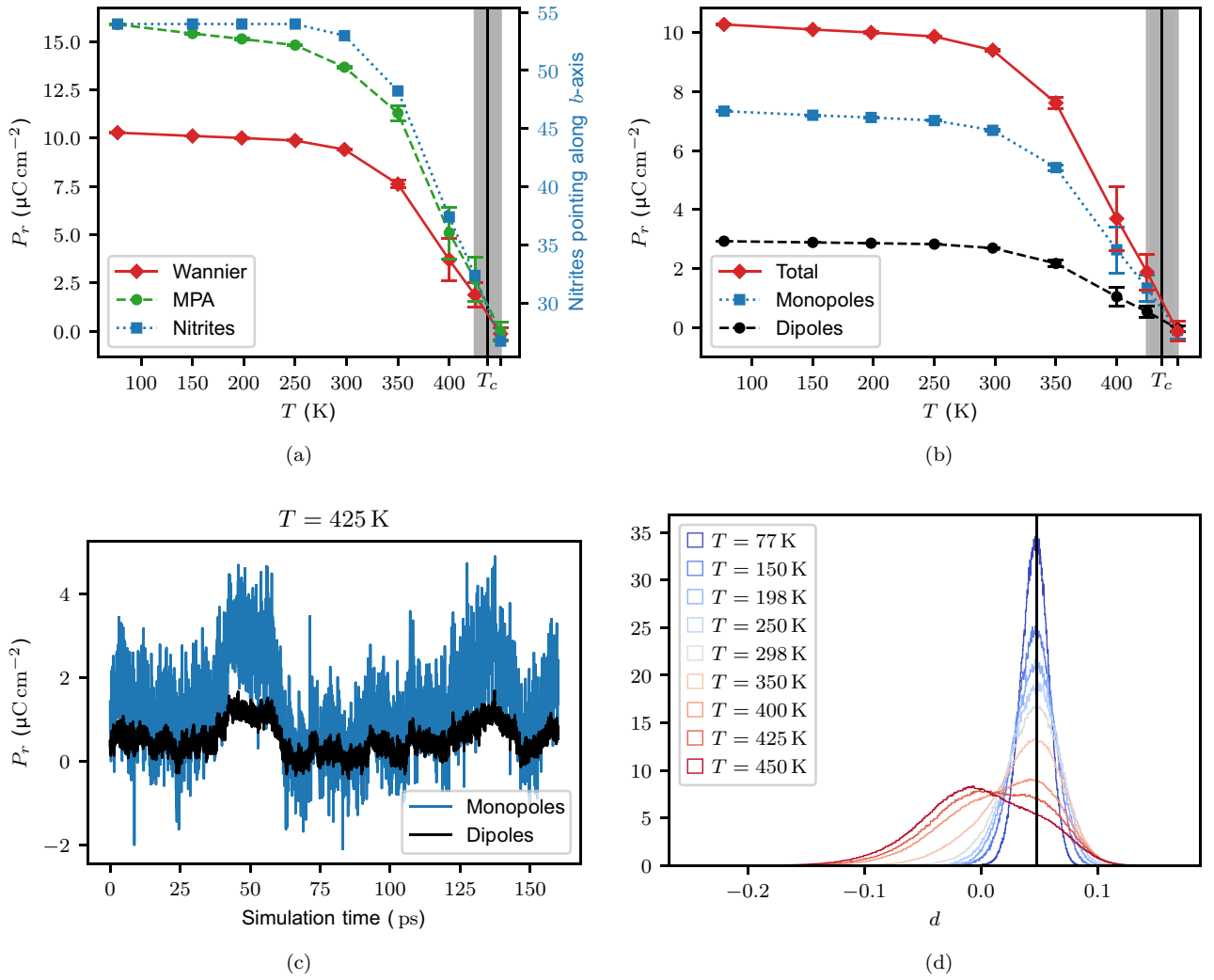

FIG. 3. (a) Evolution of the remnant polarization P_r with increasing temperature, based on the MPA charges and MLWFs. In addition, the number of nitrite ions pointing along the b direction is plotted. (b) Evolution of the remnant polarization by means of the monopole and dipole contributions with increasing temperature based on the MLWFs. (c) The monopole and dipole contributions to the remnant polarization are plotted along the trajectory at 425 K. (d) Histograms of the displacements d of cations and anions in the 1D chain of Fig. 1 along the trajectories. The black vertical line corresponds to the displacements in the starting structure. The gray shaded areas in (a) and (b) mark the range in which T_c lies. The vertical lines mark the experimental value for T_c. To give an impression for the sampling error, $\pm 2\sigma$ is plotted as statistical error.

defined as

$$\vec{\mu} = \sum_i q_i(\vec{r}_i - \vec{r}_{\text{com}}), \tag{1}$$

where the sum runs over the corresponding atoms and Wannier centers i, q_i is the charge of the atom or Wannier center, $\vec{r}_i$ is the position of the atom or Wannier center, and $\vec{r}_{\text{com}}$ is the center of mass of the ionic species. The total polarization $\vec{P}$ is obtained by dividing the cell dipole moment by the cell volume Ω:

$$\vec{P} = \frac{1}{\Omega}\sum_i q_i \vec{r}_i, \tag{2}$$

where the sum runs over all atoms and Wannier centers in the simulation cell. The remnant polarization P_r is defined in the following as polarization along the b axis P_b.

III. RESULTS AND DISCUSSION

A. Evolution of remnant polarization and lattice parameters

With increasing temperature, P_r is decreasing, as shown in Fig. 3(a). At 77 K, MPA predicts a remnant polarization of 15.9 μC cm^{-2}, overestimating the experimental value of 11.7 μC cm^{-2} [29] by 36%. In contrast, the remnant polarization based on the MLWFs ($P_r = 10.3$ μC, cm^{-2}) underestimates the experimental value by 12%. Note, however, that the simulations predict a by 8% higher unit cell volume in comparison to the experimental value (see Fig. 4). Taking this into account, we can calculate the dipole moment per unit cell, resulting in $\mu_b = 3.5$ D for the Wannier centers, which compares quite well with the experimental value of $\mu_b = 3.6$ D. This demonstrates that a Wannier center analysis delivers results in good agreement with both the experimental observations and theoretical predictions from berry phase

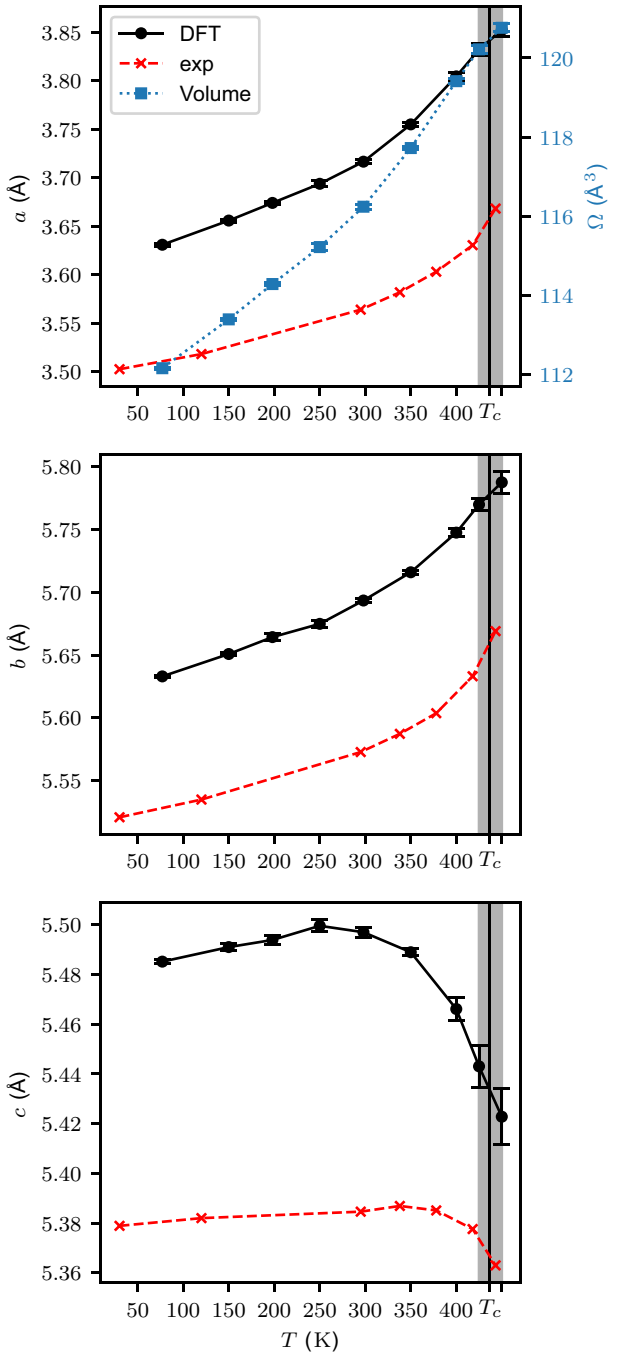

FIG. 4. Evolution of the lattice constants with increasing temperature. Experimental values are based on the studies by Gohda *et al.* [48–50], Okuda *et al.* [51], and Komatsu *et al.* [52]. The top figure shows the evolution of lattice constant a and volume Ω (computed from our simulations), the middle panel lattice constant b and the lower one lattice constant c. To give an impression for the sampling error, $\pm 2\sigma$ is plotted as statistical error. The gray shaded area marks the range in which T_c lies. In addition the experimental Curie temperature is sketched.

calculations, whereas the MPA based values severely overestimate P_r, as already shown by Alfredsson and coworkers [27]. It should also be noted that the shape of the P_r versus temperature curves differ for the localization methods. Whereas P_r in case of the Wannier analysis decays almost linearly until 300 K, the values of P_r based on the MPA decays linearly only until 250 K. Thus the transition range ΔT of the latter is 200 K wide, whereas the Wannier localization technique predicts a transition window of only 150 K. In experimental measurements the transition is always steeper with a range of maximum 50 K [29].

The theoretical simulations predict a Curie temperature T_c between 425 K and 450 K (gray shaded area in Fig. 3), being in excellent agreement with the experimental value of 437 K. In addition, Fig. 3 shows the average number of nitrite ions pointing along the same direction with respect to the b axis. At $T = 77$ K, all 54 ions are oriented in the same direction, whereas at $T = 450$ K, in average, 27 ions point upwards and 27 point downwards in accordance with a order-disorder phase transition. Interestingly, already at $T = 298$ K, still in the ferroelectric regime, we observe the appearance of disorder, namely by one nitrite ion pointing in the opposite direction in comparison to the other 53.

As already pointed out in the introduction, the remnant polarization P_r stems not only from the ordering of the nitrite ions but also from a translation of the sodium ions relative to the nitrites. To shed light on this behavior, the total remnant polarization P_r was split up into monopole and dipole contributions. For this purpose, the Wannier picture was maintained: every sodium ion was associated with a charge of $+1$ e, and every nitrite ion with a charge of -1 e. Furthermore it was assumed that the center of charge is equal to the center of mass. By applying Eq. (2) only to the monopoles, the contribution of the monopoles to the total remant polarization was calculated. The dipole contribution was computed by adding up the dipole moments of the nitrite ions based on the centers of the MLWFs. Figure 3(b) shows the evolution of the total remnant polarization and the respective monopole and dipole contributions, whereas the actual values of these contributions depend on the choice of the center of charge. It can be seen that both monopoles and dipoles contribute to the total polarization and that they decay in an almost parallel manner. That does not only apply to the thermal average but also to their time evolution. Figure 3(c) displays the evolution of the monopole and dipole contributions along the trajectory at 425 K. They evolve in phase to each other, indicating the strong coupling between both contributions.

Moreover, the monopole contribution to the total remnant polarization can be abstracted into one-dimensional chains of alternating cations and anions as depicted in Fig. 1. Such a chain is unpolarized when the distance between the ions amounts to $\frac{1}{2}b$, where b is the lattice constant of the one-dimensional ionic chain and is in this case equal to lattice parameter b. As shown by Spaldin, the polarization of such a system can be expressed as a linear function of the displacement d from the distance $\frac{1}{2}b$ of the cations/anions relative to the anions/cations [31]. Figure 3(d) show histograms of the displacement d in fractional coordinates for the investigated temperatures. The distribution becomes broader at higher temperatures but remains unimodal, indicating a displacive phase transition for the monopole contribution. For $T > T_c$, the distribution does not center exactly at $d = 0$ since the center of the heterogenous nitrite charge distribution was approximated with its center of mass.

The decomposition of the total remnant polarization in monopole and dipole contributions leads to the conclusion that the phase transition in $NaNO_2$ is not of a pure order-disorder nature. Instead, it is a combined displacive order-disorder phase transition. Whereas the nitrite ions exhibit order-disorder characteristics, the sublattice of monopoles undergoes a displacive phase transition, as already pointed out experimentally by Ichikawa *et al.* [47].

The evolution of the lattice parameters a, b, and c with increasing temperature in comparison to XRD measurements by Gohda *et al.* [48–50], Okuda *et al.* [51], and Komatsu and coworkers [52] is shown in Fig. 4. In addition, the average cell angles are displayed in Ref. [45] (Fig. S2). The orthorhombic shape is preserved during the phase transition. As already mentioned, our simulations overestimate the unit cell parameters and the unit cell volume Ω. a, b, and Ω are increasing linearly until 300 K. Above 300 K, their slope is increasing. This point coincides well with the formation of a certain amount of disorder in the cell [see Fig. 3(a)]. The lower panel of Fig. 4 shows that the lattice constant c is decreasing with increasing temperature, which was observed experimentally by Hoshino and Shibuya in 1961 [15]. The reason for this behavior can be attributed to the structure of the material. In the ferroelectric phase, the material forms –V–V– shaped chains of nitrite ions along the c axis (see Fig. 1). After the phase transition, in average half of the nitrite ions are flipped, forming a –V–Λ– shaped chain of ions, where the latter is packed closer. It should be noted that this effect is experimentally less pronounced than in our simulations. A possible reason for this discrepancy could be due to the in general higher unit cell volume in our simulations, or the use of an idealized relatively small unit cell without any defects under periodic boundary conditions. Furthermore, it catches the eye that the sampling error for lattice parameter c is larger than for a and b, which is due to the slow rotatory motion of the nitrite ions, which affects especially the c axis.

The incommensurate antiferroelectric phase was not observed in our simulations for two reasons: (i) the temperature steps between our simulations were too large for the detection of this phase being present only in a 2 K wide temperature window. Such small temperature steps would exceed our computational resources. (ii) The size of our simulation cell together with the use of periodic boundary conditions prevents the formation of an incommensurate phase. To overcome these obstacles, more efficient molecular mechanics models have to be developed to be able to simulate longer time and length scales.

B. Crystal field effect

To investigate how the phase transition alters the properties of the ionic species in the crystal, we analyzed the interionic charge transfer and the ionic dipole moments. Figure 5 shows histograms of the sodium partial charge, computed from the trajectories at different temperatures. With increasing temperature a continuous shift of the means of the distributions towards higher positive charge is observed, indicating a decrease in charge transfer with increasing temperature. This shift can be explained by the crystal structure of the material. As shown in Fig. 1, the V-shaped nitrite ions are located

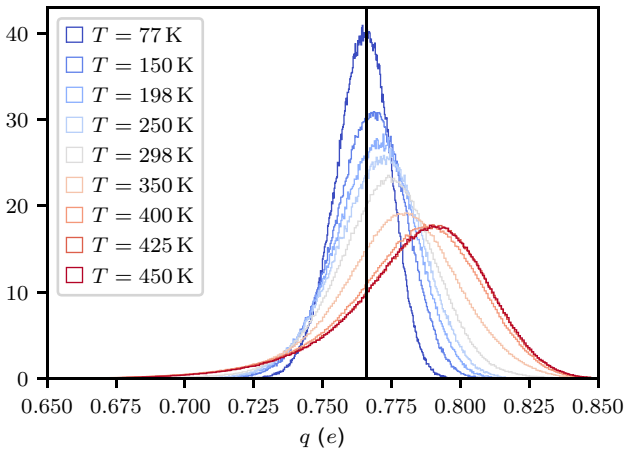

FIG. 5. Histograms of the partial charges of the sodium ions computed by MPA along the trajectories. The black vertical line corresponds to the partial charge of the sodium ion in our starting structure.

together with the sodium ions in the bc plane. In the ordered ferroelectric phase, the lone pair at the nitrogen atom (see Fig. 2) coordinates always one sodium ion, creating a transfer of electron density from the formally -1 e charged nitrite ion to the formally $+1$ e charged sodium ion. As temperature increases, more and more nitrite ions start librating, which leads to a decrease in the overlap of this lone pair with the sodium ion, resulting in a diminished charge transfer.

The dipole moments of the nitrite ions along the b axis are shown in Fig. 6. Up to 250 K, only a thermal broadening of the peak is observed. In accordance with Fig. 3, at 298 K, the first disorder emerges, which can be seen by the formation of a double peak. At 450 K, half of the nitrite ions are flipped and both peaks are evenly shaped. This formation of a double peak is expected for an order-disorder mechanism and underlines the conclusions drawn above regarding the general nature of the phase transition. Particularly interesting is the region displayed in the inset of Fig. 6, showing a zoom-in on the

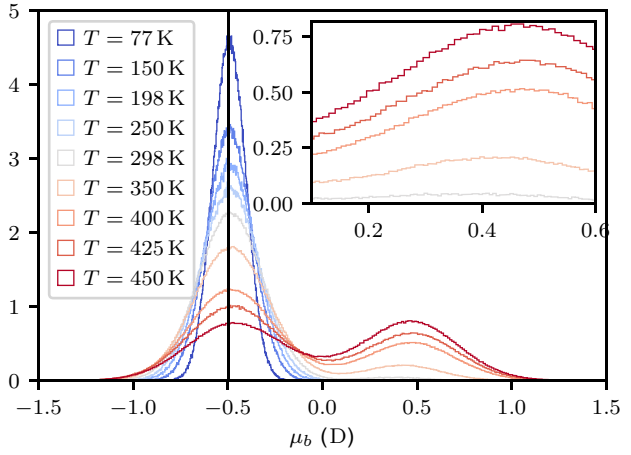

FIG. 6. Histograms of the dipole moments of the NO_2^- ions along the b axis. The black vertical line corresponds to the dipole moment in our starting structure.

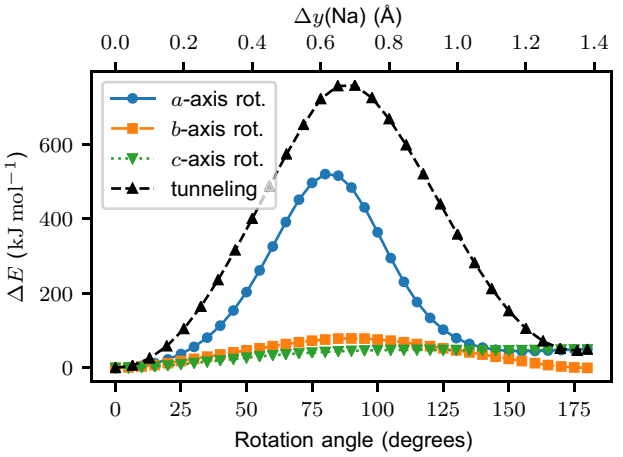

FIG. 7. Energy barriers calculated for four different motions: (i) rotation of a nitrite about the a axis ($\Delta E = 520$ kJ mol^{-1}), (ii) rotation of a nitrite about the b axis ($\Delta E = 79$ kJ mol^{-1}), (iii) rotation of the nitrite around the c axis ($\Delta E = 49$ kJ mol^{-1}), and (iv) tunneling of the N atom ($\Delta E = 757$ kJ mol^{-1}). Rotations were performed about an axis through the molecular center of mass.

formation of the double peak. With increasing temperature a shift towards higher values for μ_b is observed. This can be explained with the crystal field effect. As long as only a small fraction of NO_2^- ions is flipped, a remnant polarization P_r (see Fig. 3) is still present, creating a field polarizing the flipped ion into the opposite direction. To further quantify this effect, we used our starting structure, and rotated one of the 54 nitrites by 180° around the c axis keeping its center of mass fixed and calculated its dipole moment. Whereas the average dipole moment in the ordered phase accounts to −0.50 D (see black vertical line in Fig. 6), the dipole moment of the flipped ion was only 0.28 D. These results coincide well with the observed shift in the inset of Fig. 6 and prove the high polarizability of the nitrite ion in the material.

C. Polarization reversal mechanism

In order to shed more light on the molecular mechanism of the phase transition, it is important to understand the polarization reversal that is based on the flipping of a nitrite ion. Three different mechanisms were proposed in the literature: (i) rotation about the c axis, (ii) rotation about the a axis, and (iii) a tunneling of the nitrogen atom along the b axis [50]. In the first step, we used the starting structure and performed rotation scans of one nitrite ion around the a, b, and c axis, keeping its center of mass and all other structural parameters fixed. In addition, we performed a scan by moving the Nitrogen atom within the plane of the nitrite ion. The results, shown in Fig. 7, confirm earlier experimental and theoretical findings. The energetically most favorable path is a rotation around the c axis, whereas rotations around the a and b axis or a tunneling of the nitrogen atom are associated with higher energy barriers. The calculated barrier for the c-axis rotation is with 49 kJ mol^{-1} in good agreement to the experimentally estimated value of 40 kJ mol^{-1} [27]. Alfredsson and coworkers predicted a barrier of 68 kJ mol^{-1} from their periodic DFT calculations, employing only a single unit cell. It is expected that calculating such barriers for a single molecular ion is affected by a large size effect. Flipping one nitrite by 180° in a single unit cell accounts to the creation of an antiferroelectric phase, which is a stable phase by itself. The barrier is then located at a rotation angle of 90°. In case of a larger supercell, where only one of the 54 nitrites is flipped, and the material is still in the ferroelectric regime, the barrier is located at a rotation angle of 180°. The energy barrier for a rotation around the b axis is 79 kJ mol^{-1}, which is in reasonable agreement with a recent experimental investigation by solid state ^{17}O NMR, predicting a barrier of 68 ± 5 kJ mol^{-1} for this motion [53].

The calculation of these barriers leads to an oversimplified picture of the polarization reversal mechanism, since for example no thermal expansion of the material is taken into account. Even worse, only one center of rotation was investigated and no concerted mechanisms can be explored, although there is experimental evidence for them to be relevant [50]. To arrive at a more accurate picture of the actual polarization reversal mechanism, we investigated the mean-square atomic displacements of the atoms in our trajectories $U_{ii} = \langle u_i^2 \rangle$, where $i = 1, 2, 3$ denotes the respective displacement along the a, b, c axes. The nitrite reversal models can be associated with the following conditions: (i) rotation around the c axis: $U_{22}(N), U_{33}(N) < U_{11}(N)$ and $U_{22}(O), U_{33}(O) < U_{11}(O)$; (ii) rotation around the a axis: $U_{11}(N), U_{22}(N) < U_{33}(N)$ and $U_{11}(O), U_{33}(O) < U_{22}(O)$; and (iii) penetration of the nitrogen through two oxygen atoms: $U_{11}(N), U_{33}(N) < U_{22}(N)$ and $U_{11}(O), U_{33}(O) < U_{22}(O)$ [24,50,52]. It was found that the conditions supporting the c-axis rotation hold true both in the ferroelectric and the paraelectric phase. In addition, it was observed that $U_{33}(Na), U_{22}(Na) < U_{11}(Na)$ holds below T_c and $U_{33}(Na), U_{11}(Na) < U_{22}(Na)$ is valid above T_c. Ichikawa *et al.* related this behavior to the partially displacive character of the phase transition explained above [47]. In Fig. 8, the mean-square atomic displacements from our simulations are shown together with the experimental results. For sodium, the experimental trends are reproduced including even the reversal in magnitudes of $U_{11}(Na)$ and $U_{22}(Na)$ at T_c. For nitrogen and oxygen, experimental trends are only reproduced up to 350 K. Above these temperatures, the sampling error gets too large to derive any reasonable trend, at least for nitrogen and oxygen. The error was estimated by computing U_{ii} for every atomic species and calculating the standard deviation from these data. The error gets this large in the temperature range of the phase transition, because the sampling time is not long enough to ensure that every nitrite flipped equally often. To solve this problem, much longer simulation times would be necessary which is not feasible at this level of theory. Interestingly our simulations show in accordance to experimental findings a characteristic increase of U_{22} with temperature. U_{22} behaves like U_{33} at lower temperatures and gets closer to the behavior of U_{11} when T_c is approached. This indicates a strong coupling between the translational motion of the nitrites and sodiums along the b axis, and the rotational motion around the c axis, resulting in a lowering of the flip activation energy with respect to the barriers calculated above [50]. In general the mean-square atomic displacements together with the calculated rotation barriers confirm the model of a c-axis rotation.

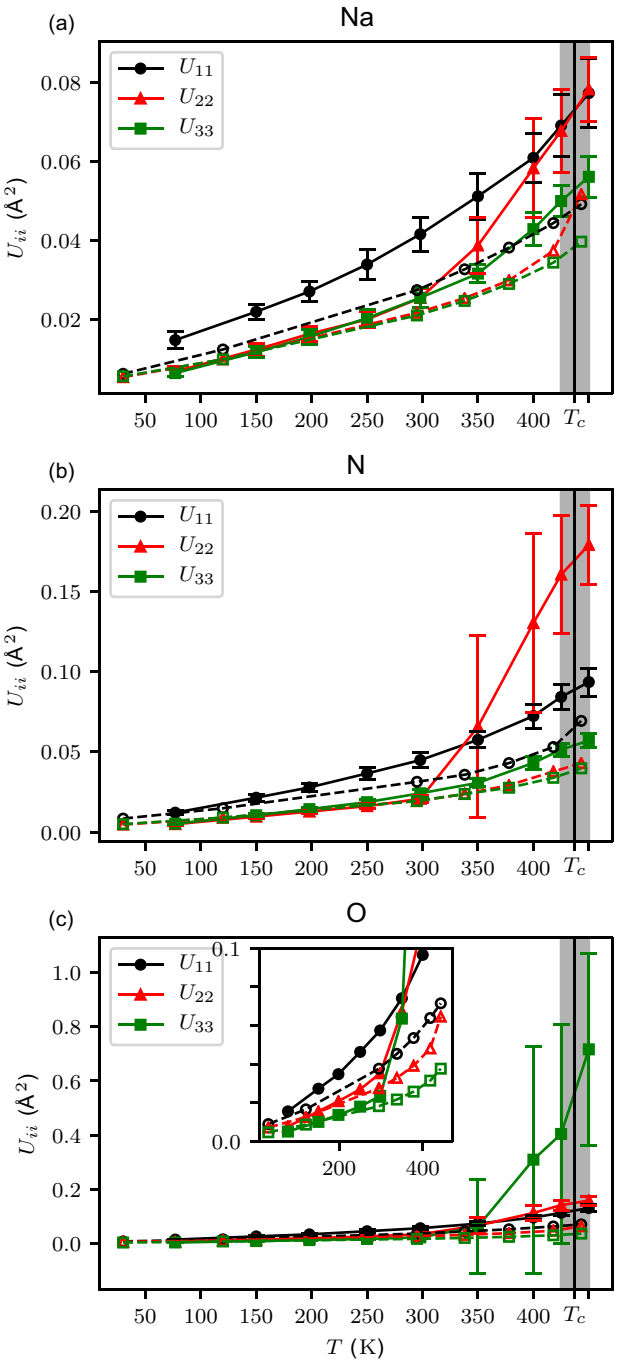

FIG. 8. Diagonal elements of the mean-square atomic displacements U_{ii} vs temperature T. (a) Na, (b) N, and (c) O atoms, respectively. Filled markers and solid lines represent the simulation results, whereas dotted lines and empty markers represent experimental findings [48–52]. The statistical error on the simulation results was estimated by computing U_{ii} for every atomic species and calculating the standard deviation from this data. For visual reasons, only $\pm\sigma$ is plotted as statistical error. The gray shaded area marks the range in which T_c lies. In addition, the experimental Curie temperature is sketched.

D. Activation energy

To quantify the decrease in the flipping activation energy E_a outlined above, we determined the flipping rate by counting the number of flips per ps per nitrite k for the trajectories at 350, 400, 425, and 450 K. These data are shown as an Arrhenius plot in Fig. 9. Performing a linear regression through all data points results in an activation energy of 36 kJ mol^{-1}, which is significantly lower than the calculated barrier of 49 kJ mol^{-1} and closer to the experimentally estimated value of 40 kJ mol^{-1} [27].

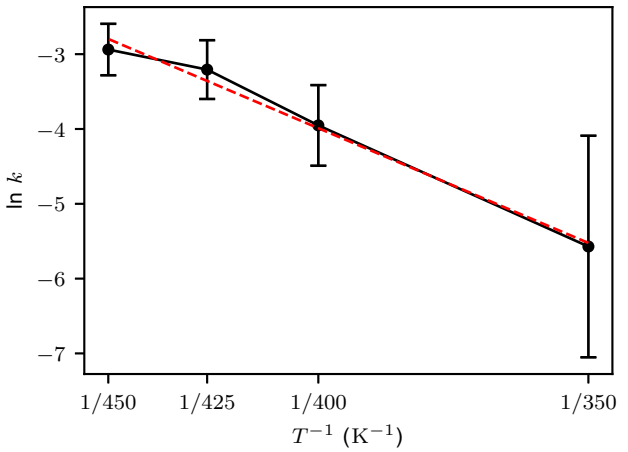

FIG. 9. Arrhenius plot of the nitrite flips per picosecond per nitrite ion in the supercell k. The statistical error was estimated by calculating the standard deviation over the flipping rates of each individual nitrite ion. For visual reasons, only $\pm\sigma$ is plotted as statistical error. The activation energy E_a in respect to the regression curve (red line) is 36 kJ mol^{-1}.

To further investigate the dependence of the activation energy on the temperature, additional simulations at different temperatures would be necessary, which is out of our computational resources.

IV. CONCLUSIONS

We performed the first *ab initio* molecular dynamics simulations of the combined displacive order-disorder phase transition of $NaNO_2$ using a dispersion corrected PBE functional. We found that the remnant polarization P_r calculated on the basis of the centers of maximally localized Wannier functions is in good agreement with experimental results. Furthermore, we were able to reproduce the experimental Curie temperature T_c and to provide new insights into the atomistic nature of the material by addressing the crystal field effect by means of interionic charge transfer and ionic dipole moments.

It can be concluded that dispersion corrected DFT employing a GGA functional using maximally localized Wannier functions to resolve the polarization, is well suited to simulate $NaNO_2$ in a quantitative fashion, where the biggest difference to experimental findings is the overestimated unit cell volume.

The insights gained in this study, together with the large amount of collected data (structures, energies, forces, stresses, charges, and dipole moments for more than 1.3 ns of simulation time) will allow us to parameterize an accurate machine learning potential for the material to simulate

longer time and length scales [54–56]. This will enable us to investigate the incommensurate phase of the material, explore its properties when incorporated into a polymer film [16,17], and to compute its electrical phase diagram [57,58], which will be of use for the further development of ferroelectric materials based on the investigated design principle.

ACKNOWLEDGMENTS

We thank Philipp Schienbein for his help with CP2K. J.P.D. is grateful for the financial support by the Fonds der Chemischen Industrie (FCI). Further financial support from the Deutsche Forschungsgemeinschaft (DFG) within the COORNETs priority program is acknowledged (grant SCHM 1389/9-1).

[1] M. E. Lines and A. M. Glass, *Principles and Applications of Ferroelectrics and Related Materials* (Oxford University Press, Oxford, 2001).

[2] N. Setter, D. Damjanovic, L. Eng, G. Fox, S. Gevorgian, S. Hong, A. Kingon, H. Kohlstedt, N. Y. Park, G. B. Stephenson, I. Stolitchnov, A. K. Taganstev, D. V. Taylor, T. Yamada, and S. Streiffer, J. Appl. Phys. **100**, 051606 (2006).

[3] J. F. Scott, Science **315**, 954 (2007).

[4] R. C. G. Naber, K. Asadi, P. W. M. Blom, D. M. de Leeuw, and B. de Boer, Adv. Mater. **22**, 933 (2010).

[5] A. von Hippel, R. G. Breckenridge, F. G. Chesley, and L. Tisza, Ind. Eng. Chem. **38**, 1097 (1946).

[6] H. Kawai, Jpn. J. Appl. Phys. **8**, 975 (1969).

[7] P.-P. Shi, Y.-Y. Tang, P.-F. Li, W.-Q. Liao, Z.-X. Wang, Q. Ye, and R.-G. Xiong, Chem. Soc. Rev. **45**, 3811 (2016).

[8] W.-Q. Liao, Y. Zhang, C.-L. Hu, J.-G. Mao, H.-Y. Ye, P.-F. Li, S. D. Huang, and R.-G. Xiong, Nat. Commun. **6**, 7338 (2015).

[9] H.-Y. Ye, W.-Q. Liao, C.-L. Hu, Y. Zhang, Y.-M. You, J.-G. Mao, P.-F. Li, and R.-G. Xiong, Adv. Mater. **28**, 2579 (2016).

[10] W. Zhang and R.-G. Xiong, Chem. Rev. **112**, 1163 (2012).

[11] K. Asadi and M. A. van der Veen, Eur. J. Inorg. Chem. **2016**, 4332 (2016).

[12] P. Jain, V. Ramachandran, R. J. Clark, H. D. Zhou, B. H. Toby, N. S. Dalal, H. W. Kroto, and A. K. Cheetham, J. Am. Chem. Soc. **131**, 13625 (2009).

[13] J. P. Dürholt, B. F. Jahromi, and R. Schmid, ACS Cent. Sci. **5**, 1440 (2019).

[14] S. Sawada, S. Nomura, S. Fujii, and I. Yoshida, Phys. Rev. Lett. **1**, 320 (1958).

[15] S. Hoshino and I. Shibuya, J. Phys. Soc. Jpn. **16**, 1254 (1961).

[16] K. C. Sekhar and R. Nath, J. Appl. Phys. **102**, 044114 (2007).

[17] K. C. Sekhar, A. Nautiyal, and R. Nath, J. Appl. Phys. **105**, 024109 (2009).

[18] K. D. Ehrhardt and K. H. Michel, Phys. Rev. Lett. **46**, 291 (1981).

[19] V. Massidda and C. R. Mirasso, J. Magn. Magn. Mater. **116**, 277 (1992).

[20] M. L. Klein and I. R. McDonald, Proc. R. Soc. Lond. A **382**, 471 (1982).

[21] M. L. Klein, I. R. McDonald, and Y. Ozaki, Phys. Rev. Lett. **48**, 1197 (1982).

[22] R. M. Lynden-Bell, M. L. Klein, and I. R. McDonald, Z. Phys. B: Condens. Matter **54**, 325 (1984).

[23] R. M. Lynden-Bell, R. W. Impey, and M. L. Klein, Chem. Phys. **109**, 25 (1986).

[24] W.-G. Yin, C.-G. Duan, W. N. Mei, J. Liu, R. W. Smith, and J. R. Hardy, Phys. Rev. B **68**, 174106 (2003).

[25] F. Ishii and T. Oguchi, J. Phys. Soc. Jpn. **71**, 336 (2002).

[26] B. Andriyevsky, Comput. Mater. Sci. **50**, 1169 (2011).

[27] M. Alfredsson, K. Hermansson, and R. Dovesi, Phys. Chem. Chem. Phys. **4**, 4204 (2002).

[28] K. Hamano, J. Phys. Soc. Jpn. **35**, 157 (1973).

[29] W. Buchheit and J. Petersson, Solid State Commun. **34**, 649 (1980).

[30] J. VandeVondele, M. Krack, F. Mohamed, M. Parrinello, T. Chassaing, and J. Hutter, Comput. Phys. Commun. **167**, 103 (2005).

[31] N. A. Spaldin, J. Solid State Chem. **195**, 2 (2012).

[32] W. Koch and M. C. Holthausen, *A Chemist's Guide to Density Functional Theory*, 2nd ed. (Wiley-VCH, Weinheim, 2001).

[33] D. Marx and J. Hutter, *Ab Initio Molecular Dynamics: Basic Theory and Advanced Methods* (Cambridge University Press, Cambridge, 2009).

[34] J. P. Perdew, K. Burke, and M. Ernzerhof, Phys. Rev. Lett. **77**, 3865 (1996).

[35] S. Grimme, J. Antony, S. Ehrlich, and H. Krieg, J. Chem. Phys. **132**, 154104 (2010).

[36] J. VandeVondele and J. Hutter, J. Chem. Phys. **127**, 114105 (2007).

[37] S. Goedecker, M. Teter, and J. Hutter, Phys. Rev. B **54**, 1703 (1996).

[38] C. Hartwigsen, S. Goedecker, and J. Hutter, Phys. Rev. B **58**, 3641 (1998).

[39] M. Krack, Theor Chem. Acc **114**, 145 (2005).

[40] V. Haigis, Y. Belkhodja, F.-X. Coudert, R. Vuilleumier, and A. Boutin, J. Chem. Phys. **141**, 064703 (2014).

[41] A. Jain, S. P. Ong, G. Hautier, W. Chen, W. D. Richards, S. Dacek, S. Cholia, D. Gunter, D. Skinner, G. Ceder, and K. A. Persson, APL Mater. **1**, 011002 (2013).

[42] K. Persson, Materials Data on $NaNO_2$ (SG:44) by Materials Project, doi:10.17188/1204127.

[43] G. Bussi, D. Donadio, and M. Parrinello, J. Chem. Phys. **126**, 014101 (2007).

[44] G. J. Martyna, D. J. Tobias, and M. L. Klein, J. Chem. Phys. **101**, 4177 (1994).

[45] See Supplemental Material at http://link.aps.org/supplemental/10.1103/PhysRevMaterials.3.094408 for the time evolution of the remnant polarization at the investigated temperatures and the average lattice angles.

[46] H. Flyvbjerg and H. G. Petersen, J. Chem. Phys. **91**, 461 (1989).

[47] M. Ichikawa, T. Gustafsson, and I. Olovsson, Solid State Commun. **123**, 135 (2002).

[48] T. Gohda, M. Ichikawa, T. Gustafsson, and I. Olovsson, J. Korean Phys. Soc. **29**, 551 (1996).

[49] T. Gohda, M. Ichikawa, T. Gustafsson, and I. Olovsson, Acta Cryst B **56**, 11 (2000).

[50] T. Gohda, M. Ichikawa, T. Gustafsson, and I. Olovsson, Phys. Rev. B **63**, 014101 (2000).

[51] M. Okuda, S. Ohba, Y. Saito, T. Ito, and I. Shibuya, Acta Cryst. **46**, 343 (1990).
[52] K. Komatsu, K. Itoh, and E. Nakamura, J. Phys. Soc. Jpn. **57**, 2836 (1988).
[53] Y. Dai, I. Hung, Z. Gan, and G. Wu, Concepts Magnetic Resonance Part A **45A**, e21409 (2016).
[54] J. Behler, J. Chem. Phys. **145**, 170901 (2016).
[55] J. Behler, Int. J. Quantum Chem. **115**, 1032 (2015).
[56] A. P. Bartók and G. Csányi, Int. J. Quantum Chem. **115**, 1051 (2015).
[57] M. Stengel, N. A. Spaldin, and D. Vanderbilt, Nat. Phys. **5**, 304 (2009).
[58] M. Stengel and J. Íñiguez, Phys. Rev. B **92**, 235148 (2015).